Vibronic Effects in Single Molecule Conductance: First-Principles Description and Application to Benzenealkanethiolates between Gold Electrodes

C. Benesch,[†] M. Čížek,[‡] J. Klimeš,[‡] I. Kondov,[†,§] M. Thoss,*[,†] and W. Domcke[†]

Department of Chemistry, Technical University of Munich, Lichtenbergstr. 4, D-85747 Garching, Germany, and Faculty of Mathematics and Physics, Institute of Theoretical Physics, Charles University, Prague, Czech Republic

The effect of vibrational motion on resonant charge transport through single molecule junctions is investigated. The study is based on a combination of first-principles electronic structure calculations to characterize the system and inelastic scattering theory to calculate transport properties. The extension of the methodology to describe hole transport through occupied molecular orbitals is discussed. The methodology is applied to molecular junctions where a benzene molecule is connected via alkanethiolate bridges to two gold electrodes. The results demonstrate that, depending on the coupling between the electronic π-system of the benzene ring and the gold electrodes, vibronic coupling may have a significant influence on the transport properties of the molecular junction.

I. Introduction

Recent advances in experimental studies of single molecule conduction[1–9] have stimulated great interest in the basic mechanisms which govern electron transport through nanoscale molecular junctions.[10–12] An interesting aspect that distinguishes molecular conductors from mesoscopic semiconductor devices is the possible influence of the nuclear degrees of freedom of the molecular bridge on electron transport. Due to the small size of molecules, the charging of the molecular bridge is often accompanied by significant changes of the nuclear geometry. The current-induced excitation of the vibrations of the molecule may result in heating of the molecular bridge and possibly breakage of the junction. Conformational changes of the geometry of the conducting molecule are possible mechanisms for switching behavior and negative differential resistance.[13] Furthermore, the observation of vibrational structures in conduction measurements allows the unambiguous identification of the molecular character of the current.

Vibrational structures in molecular conductance were observed, for example, in electron transport experiments on H_2, HD, and D_2 between platinum electrodes[14] using the mechanically controllable break junction technique. Thereby, changes in the conductance were assigned to switching between two different local geometrical configurations induced by the transverse motion of the molecule. The observed vibrational structures could be classified as longitudinal or transversal.[15] In studies of C_{60} molecules between gold electrodes,[2] the center of mass motion of the molecular bridge was observed. Other experiments on this system[16,17] as well as on C_{70},[7] $(C_{70})_2$,[18] and copper phtalocyanin[6] on an aluminum oxide film showed structures which were related to the internal vibrational modes of the molecule. The aluminum oxide layer in the latter experiment acted as an insulating layer, which effectively reduces the electronic coupling between the molecule and the

metal substrate thus facilitating the effect of vibrational motion on the conductance. In another STM experiment,[19] pronounced progressions of vibrational modes were observed and the dependence of the vibronic coupling on the spatial position of the STM tip was demonstrated. Moreover, vibrational signatures of molecular bridges have also been observed in off-resonant inelastic electron tunneling spectroscopy (IETS).[20,21]

This tremendous experimental progress has inspired great interest in the theoretical modeling and simulation of vibrationally coupled electron transport in molecular junctions.[22–39] In the low-voltage, off-resonant transport regime, combinations of electronic-structure calculations and nonequilibrium Green's function theory (NEGF), employing the self-consistent Born approximation (SCBA), have been used to investigate vibrational signatures in IETS.[26–28] Other approaches used to describe inelastic features in the off-resonant region include scattering theory combined with an expansion of either the molecular Green's function to first order in vibronic interaction[29] or the systems wave function in the nuclear coordinates.[30]

The majority of the studies of vibronic effects in the resonant tunneling regime (for higher voltages) have been based on generic tight-binding models, using an NEGF approach based on the equation of motion method on the Keldysh contour[31] or kinetic rate equations to calculate the current.[32–37] These model studies have demonstrated that the vibrational motion of the molecular bridge may affect the current–voltage characteristics significantly.

Many of the studies of vibrationally coupled electron transport reported so far invoke approximations which restrict their applicability either to small electronic–vibrational coupling, small molecule–lead coupling, or separability of the vibrational modes. We have recently proposed an approach,[40,41] which is based on inelastic multichannel scattering theory and the projection–operator formalism of resonant electron–molecule scattering.[42] Within this scattering theory approach, the inelastic transmission probability of a single electron is calculated numerically exactly, whereas the current is described approximately using an inelastic extension of the Landauer

* To whom correspondence should be addressed.
† Technical University of Munich.
‡ Charles University.
§ Present address: Forschungszentrum Karlsruhe, Herrmann-von-Helmholtz-Platz 1, 76344 Eggenstein-Leopoldshafen, Germany.

Vibronic Effects in Single Molecule Conductance

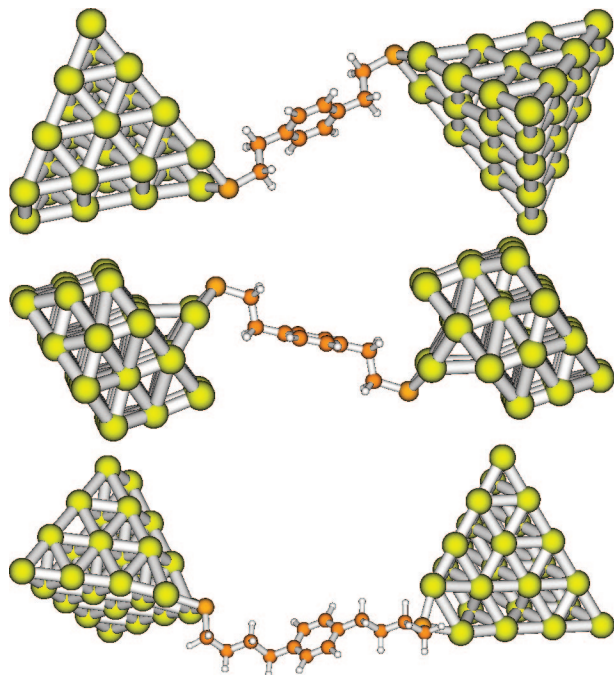*J. Phys. Chem. C, Vol. 112, No. 26, 2008* **9881**

Figure 1. Three molecular junctions investigated: benzene-di(ethanethiolate) (BDET) between pyramidal gold contacts (top), BDET between cuboid-shaped gold contacts (middle), and benzene-di(butanethiolate) (BDBT) between pyramidal gold contacts (bottom).

formula.[60] Closely related scattering theory approaches have been proposed by Bonca and Trugman[38] and Ness et al.[39]

In previous work,[40,41] we have applied this formalism to study vibronic effects in molecular conductance based on generic models for molecular junctions. In a recent short communication,[43] we have combined the scattering theory approach with first-principles electronic-structure calculations to characterize the molecular junction. In this paper, we give a detailed description of the methodology including a derivation of the model Hamiltonian for hole transport, a description of the partitioning method used to determine the parameters of the Hamiltonian by first-principles electronic structure calculations, and an outline of the scattering theory approach. The methodology is applied to study vibronic effects on conductance in molecular junctions where a benzene ring is connected via alkanethiol bridges to two gold electrodes ($Au-S-(CH_2)_n-C_6H_4-(CH_2)_n-S-Au$, cf. Figure 1). This class of molecular junctions was chosen, because the change of the length of the alkyl chain, n, allows a systematic variation of the coupling between the electronic π-system of the phenyl ring and the gold electrodes and thus a variation of the lifetime of the electron on the molecular bridge. Our previous studies show that, due to the strong molecule lead coupling, benzenethiolate (corresponding to $n = 0$) between gold electrodes exhibits only minor vibronic effects.[43] In this work, we consider benzene-di-(ethanethiolate) ($n = 2$) and benzene-di(butanethiolate) ($n = 4$), which correspond to moderate and weak molecule-lead coupling, respectively.

II. Theory

A. Charge Transport Model Hamiltonian. To study charge transport through single molecule junctions employing inelastic scattering theory, we use an effective single-particle model Hamiltonian with parameters determined by first-principles electronic structure calculations. In this section we briefly outline the derivation of the Hamiltonian.

The Hamiltonian of a metal−molecule−metal (MMM) junction including the electronic-nuclear interaction is given by the generic expression (we use atomic units where $\hbar = e = 1$)

$$H = T_n + V_{nn}(\mathbf{R}) + H_e(\mathbf{R}) \tag{2.1}$$

Here T_n denotes the kinetic energy of the nuclei,

$$T_n = \sum_a \frac{\mathbf{p}_a^2}{2M_a} \tag{2.2}$$

where $\mathbf{p}_a$ is the momentum and M_a is the mass of nucleus a. The Coulomb interaction of the nuclei is given by

$$V_{nn}(\mathbf{R}) = \sum_{a \neq b} \frac{Z_a Z_b}{|\mathbf{R}_a - \mathbf{R}_b|} \tag{2.3}$$

where Z_a is the atomic number and $\mathbf{R}_a$ denotes the Cartesian coordinates of the position of nucleus a. The electronic Hamiltonian, $H_e(\mathbf{R})$ includes the kinetic energy and the Coulomb interaction of the electrons as well as the electronic-nuclear Coulomb interaction and depends parametrically on the nuclear coordinates $\mathbf{R}$.

We first focus on the electronic degrees of freedom and consider the equilibrium situation without bias voltage at zero temperature. In this case, the junction is in its electronic ground state. Employing an effective one particle description, the ground-state is given by a single Slater determinant, $|\Psi_g\rangle = \prod_{i=1}^{n_{el}} c_i^\dagger |0\rangle$, where $|0\rangle$ denotes the vacuum state, the operator $c_i^\dagger$ creates an electron in the single particle state (molecular orbital) i and the product is taken over all n_{el} electrons in the neutral junction. $|\Psi_g\rangle$ is an approximate solution of the electronic Schrödinger equation

$$H_e(\mathbf{R})|\Psi_g\rangle = E_g(\mathbf{R})|\Psi_g\rangle \tag{2.4}$$

with energy $E_g(\mathbf{R})$, which parametrically depends on the nuclear coordinates. The energy $E_g(\mathbf{R}) + V_{nn}(\mathbf{R})$ represents the adiabatic potential energy surface of the electronic ground state, which will serve as a reference state in the following.

If an external voltage is applied to the MMM junction, electrons (or holes) are transferred from an external reservoir to the junction and vice versa; that is, the number of electrons on the junction, n_{el}, will change. Here we consider charge transfer processes which result in one additional electron (corresponding to the anion) or one additional hole (corresponding to the cation) on the junction. Within Koopmans' theorem, the energy of a cation is given by subtracting the energy of the single-particle state (molecular orbital), from which the electron was removed, from the energy of the neutral ground state. The energy of an anion, on the other hand, is given by adding the energy of the single-particle state that was occupied to the energy of the neutral ground state. An electronic Hamiltonian that can describe both situations is given by[44]

$$H_e(\mathbf{R}) = E_g(\mathbf{R}) - \sum_{j \in occ} E_j(\mathbf{R}) c_j c_j^\dagger + \sum_{i \in unocc} E_i(\mathbf{R}) c_i^\dagger c_i \tag{2.5}$$

where the index j labels all orbitals that are occupied in the neutral reference state, whereas the index i labels all orbitals that are unoccupied in the neutral reference state. Thereby, effects due to electron−electron correlation and orbital relaxation have been neglected.[45] It is also noted that the restriction to charge transfer processes that change the number of electrons on the junction by at most one is expected to be valid for a finite MMM junction with molecular character (see below) and not too large voltages.

If the electronic spectrum of a molecular junction is such that the levels, which contribute to conduction, are all located far below or far above the Fermi energy, the third or second term in eq 2.5 can be neglected, respectively. In the latter case, the current is dominated by electron transport, whereas in the former case, hole transport prevails. Thus, in the two limiting cases, we obtain the electronic Hamiltonian

$$H_e(\mathbf{R}) = E_g(\mathbf{R}) + \sum_i E_i(\mathbf{R}) c_i^\dagger c_i \qquad (2.6a)$$

$$H_e(\mathbf{R}) = E_g(\mathbf{R}) - \sum_j E_j(\mathbf{R}) c_j c_j^\dagger \qquad (2.6b)$$

for electron or hole transport, respectively. In all applications considered below, the transport is dominated by hole transport. Therefore, we will consider in the following only this case. A more detailed discussion and comparison of both cases is given in ref 46.

To describe charge transport trough a molecular junction, it is expedient to partition the overall system into the molecule and the left and right leads. As will be described in more detail in section II.B, this results in a splitting of the second term in eq 2.6b into three terms, describing the molecule, the left electrode, and the right electrode separately

$$H_e(\mathbf{R}) = E_g(\mathbf{R}) - \sum_{m \in M} E_m(\mathbf{R}) c_m c_m^\dagger - \sum_{k \in L,R} E_k c_k c_k^\dagger -$$
$$\sum_{m \in M} \sum_{k \in L,R} (V_{mk} c_k c_m^\dagger + V_{km} c_m c_k^\dagger) \qquad (2.7)$$

Here the indices m and k denote orbitals that are either localized on the molecule (M), or on the left (L) or right (R) lead, respectively, $c_m^\dagger$ and $c_k^\dagger$ are the corresponding creation operators, and V_{mk} describes the coupling between molecule and leads. In eq 2.7, we have assumed that direct interactions between the left and right lead can be neglected and that the energies of the lead states E_k, as well as the coupling matrix elements, V_{mk}, are approximately independent of the nuclear coordinates.[47] As a result, for transport calculations, the distinction between electron and hole transport is only necessary for the orbitals localized on the molecule. In particular, the Hamiltonian (2.7) is equivalent to

$$\widetilde{H}_e(\mathbf{R}) = \widetilde{E}_g(\mathbf{R}) - \sum_{m \in M} E_m(\mathbf{R}) c_m c_m^\dagger + \sum_{k \in L,R} E_k c_k^\dagger c_k +$$
$$\sum_{m \in M} \sum_{k \in L,R} (V_{km} c_k^\dagger c_m + V_{mk} c_m^\dagger c_k) \qquad (2.8)$$

with the renormalized ground-state energy

$$\widetilde{E}_g(\mathbf{R}) = E_g(\mathbf{R}) - \sum_{k \in L,R} E_k \qquad (2.9)$$

Unlike for the orbitals localized on the molecule, which have energies $E_m(\mathbf{R})$ that depend on the nuclear geometry $\mathbf{R}$, the constant shift $\sum_{k \in L,R} E_k$ in eq 2.9 has no influence on the dynamics and on transport properties. Similarly, increasing the number of electronic states in the leads by including a larger portion of the electrodes in the extended molecule will only change the density of sampling of the continuum states E_k and shift $E_g(\mathbf{R})$ by an $\mathbf{R}$-independent constant that is irrelevant for transport calculations. Thus, in contrast to eq 2.6b, which describes a finite system, the Hamiltonian (2.7) can be used to describe the overall system including the infinite leads.

In the applications considered below, we use the harmonic approximation for the nuclei. In this approximation, the potential energy of the nuclei in the electronic ground state, $E_g(\mathbf{R}) + V_{nn}(\mathbf{R})$, is expanded up to second order in the nuclear coordinates around the equilibrium geometry ($\mathbf{R}_{eq}$) of the neutral molecule. This results in the following expression for the nuclear Hamiltonian of the neutral reference state

$$T_n + V_{nn}(\mathbf{R}) + E_g(\mathbf{R}) = H_{n0} = \sum_l \omega_l \left(a_l^\dagger a_l + \frac{1}{2} \right) \qquad (2.10)$$

where ω_l is the frequency of the lth vibrational normal mode of the molecule with dimensionless coordinate q_l and $a_l^\dagger$ and a_l denote the corresponding creation and annihilation operators. Employing, furthermore, an expansion of the molecular energies $E_j(\mathbf{R})$ up to first order around the equilibrium geometry of the neutral molecule, the overall Hamiltonian for hole transport is given by

$$H = \sum_l \omega_l \left(a_l^\dagger a_l + \frac{1}{2} \right) - \sum_{m \in M} E_m c_m c_m^\dagger - \sum_{l, m \in M} \frac{\kappa_l^{(m)}}{\sqrt{2}} (a_l + a_l^\dagger) c_m c_m^\dagger -$$
$$\sum_{k \in L,R} E_k c_k c_k^\dagger + \sum_{m \in M} \sum_{k \in L,R} (V_{mk} c_m^\dagger c_k + V_{km} c_k^\dagger c_m) \qquad (2.11)$$

Here, we have introduced the electronic-vibrational (vibronic) coupling parameters

$$\kappa_l^{(m)} = \left(\frac{\partial E_m}{\partial q_l} \right)_{R_{eq}} \qquad (2.12)$$

The linear form of the vibronic coupling implies that only normal modes belonging to the totally symmetric representation of the respective symmetry group have a nonvanishing coupling constant. The harmonic approximation of the nuclear potential employed in eq 2.11 is valid for small amplitude motion around the equilibrium geometry. For a treatment of large amplitude (e.g., torsional) motion in molecular junctions, see ref 41.

In this paper, the Hamiltonian derived above is used in combination with inelastic scattering theory to study inelastic charge transport. When employing scattering theory, it is expedient to represent the Hamiltonian in terms of effective single-particle states for the electronic degrees of freedom. In the case of hole transport, the relevant single particle states are $|\phi_m\rangle = c_m|\Psi_g\rangle$, $|\phi_k\rangle = c_k|\Psi_g\rangle$, which describe an additional hole on the molecule or the leads, respectively. The effective single-particle representation of the Hamiltonian is obtained by projecting eq 2.11 onto the single-particle space, i.e., $H \rightarrow \sum_{i, i'} |\phi_i\rangle\langle\phi_i|H|\phi_{i'}\rangle\langle\phi_{i'}|$ This results in

$$H = H_{n0} - H_M - H_{ne} - H_L - H_R - V \qquad (2.13)$$

with

$$H_{n0} = \sum_l \omega_l \left(a_l^\dagger a_l + \frac{1}{2} \right) \qquad (2.14a)$$

$$H_M = \sum_{m \in M} |\phi_m\rangle E_m \langle\phi_m| \qquad (2.14b)$$

$$H_{ne} = \sum_{l, m \in M} \frac{\kappa_l^{(m)}}{\sqrt{2}} (a_l + a_l^\dagger) |\phi_m\rangle \langle\phi_m| \qquad (2.14c)$$

$$H_L + H_R = \sum_{k \in L,R} |\phi_k\rangle E_k \langle\phi_k| \qquad (2.14d)$$

$$V = \sum_{m \in M} \sum_{k \in L,R} (|\phi_m\rangle V_{km} \langle\phi_k| + |\phi_k\rangle V_{mk} \langle\phi_m|) \qquad (2.14e)$$

The negative signs in eq 2.13 are due to the fact that we consider hole transport. The Hamiltonian for electron transport

Vibronic Effects in Single Molecule Conductance

J. Phys. Chem. C, Vol. 112, No. 26, 2008 **9883**

can be derived in a similar way and is explicitly given in ref 46. It is noted, that for purely electronic transport calculations (i.e., without vibronic coupling, $\kappa_l^{(m)} = 0$), the different Hamiltonians for electron and hole transport give the same current−voltage characteristic. Including vibronic coupling, this is, however, no longer the case.[46]

B. First-Principles Determination of Parameters. The parameters of the Hamiltonian (2.13) describing the molecular junction are determined by first-principles electronic structure calculations. To this end, the overall junction is partitioned into five parts: The molecular part, the part of the left and right electrodes that is explicitly included in the quantum chemistry calculation (in the following referred to as the contacts), and the remaining parts of the left and right electrodes. The molecule and the contacts form the extended molecule and are treated explicitly by quantum chemistry calculations. The influence of the remaining part of the electrodes is taken into account implicitly employing the surface self-energy of a gold (111) surface.

1. Electronic Structure Methods. The parameters for the explicitly calculated part of the molecular junctions were determined employing electronic-structure calculations performed with the TURBOMOLE package (V5−7)[49] using density functional theory (DFT) with the B3-LYP hybrid functional and the SV(P) basis set including ECP-60-MWB on the gold atoms.

The final structure of the three systems considered (cf. Figure 1) was the result of several optimization cycles: A full geometry optimization of the isolated neutral molecule was followed by a full geometry optimization of the system obtained after replacing the hydrogens on sulfur by two gold atoms. Covalent bonding to two gold atoms is the preferred bond formation if no symmetry constraints are applied.[4,50] Finally, a second metal layer containing five gold atoms was added on both sides and the geometry of the system was again optimized, thereby keeping the internal coordinates of the second gold layer fixed. The final geometry of the metal contacts was obtained by increasing the second layer by several atoms and/or adding two more metal layers, which are cutouts of the (111)-plain of the face-centered-cubic lattice of solid gold. A single-point DFT calculation was performed on this system. The Fermi energy was approximated by the average value of the energies of the HOMO and LUMO.

2. Partitioning Method and Electronic Parameters. The electronic structure calculations discussed above result in delocalized molecular orbitals for the extended molecule. To determine the single-particle states $|\phi_j\rangle$, $|\phi_k\rangle$ included in the Hamiltonian (2.13), which are localized on the leads or the molecule, respectively, and the corresponding electronic energies and coupling parameters, we employ a partitioning method. This method is based on the following four steps: (i) separation of the overall Hilbert space into left contact, molecule, and right contact, (ii) partitioning of the Hamiltonian according to this separation, (iii) introduction of a self-energy to describe the influence of the remaining infinite electrodes, and (iv) a separate diagonalization of the three blocks of the partitioned Hamiltonian. The detailed procedure is discussed in the following.

As was mentioned above, in the present paper we work within an effective single-electron picture. Thus we identify the effective electronic Hamiltonian with the Kohn−Sham matrix, F, of the self-consistent-field DFT calculation. The Kohn−Sham matrix is represented in a set of atomic orbitals $|\chi_n\rangle$. To separate the overall Hilbert space into three mutually orthogonal subspaces describing the molecule and the two contacts, the following projection procedure was employed: First, the set of

atomic orbitals of the overall system, $\{|\chi_n\rangle\}$ is divided into three groups, which are centered at the left contact, the molecule, and the right contact, respectively. Since it is advantageous to work with orthogonal orbitals,[51,52] the set of atomic orbitals of the overall system is orthogonalized according to Löwdin [53,54]

$$|\tilde{\chi}_n\rangle = \sum_n (S^{-1/2})_{nl}|\chi_l\rangle \quad (2.15)$$

where S denotes the atomic orbital overlap matrix with elements $S_{ln} = \langle\chi_l|\chi_n\rangle$. The new basis functions obtained, $|\tilde{\chi}_n\rangle$, exhibit a minimal deviation from the original ones in a least-squares sense, and hence, their localization is preserved. In particular, the classification into the three groups (left contact, molecule, right contact) is still valid.

The new set of orthogonal basis functions $\{|\tilde{\chi}_n\rangle\}$ is then used to partition the Kohn−Sham matrix from the converged DFT calculation into the three subspaces. The Kohn−Sham matrix in the orthogonal basis is given by

$$\widetilde{F} = S^{-1/2}FS^{-1/2} \quad (2.16)$$

According to the separation of the orthogonalized basis set to the three groups—left contact, molecule, and right contact—the transformed Kohn−Sham matrix can be arranged in the following block structure:

$$\widetilde{F} = \begin{pmatrix} \widetilde{F}_L & \widetilde{F}_{LM} & \widetilde{F}_{LR} \\ \widetilde{F}_{ML} & \widetilde{F}_M & \widetilde{F}_{MR} \\ \widetilde{F}_{RL} & \widetilde{F}_{RM} & \widetilde{F}_R \end{pmatrix} \quad (2.17)$$

The thus obtained Kohn−Sham matrix describes the extended molecule, which includes a part of the electrodes. To incorporate the influence of the remaining (infinite) parts of the electrodes, we use a surface Green's function technique. Within this method, the influence of the remaining part of the electrodes is described by the corresponding self-energy. Within the Green's function formalism employed below to calculate transport properties this amounts to adding the self-energy to the Kohn−Sham matrix elements belonging to the gold atoms of the outermost layer of the contacts

$$F^{tot} = \widetilde{F} + \Sigma^{sf} \quad (2.18)$$

This method to incorporate the remaining (infinite) parts of the electrodes in the description can be rigorously justified using projection operator techniques. For an outline of the derivation in the context of electron transfer at surfaces, see for example ref 56. The surface self-energy Σ^{sf} was obtained by calculating the surface Green's function for a (111) gold surface representing the semi-infinite electrode.[55] The surface Green's function of a gold (111) surface was determined using a generalization of the method developed by Sancho et al.[57] Thereby, the (111) surface of gold was described by a tight binding model.[58] Furthermore, we have neglected nondiagonal contributions, which correspond to coupling between different gold atoms. It is noted that, due to the added self-energy, the Kohn−Sham matrix is no longer real but complex symmetric.

In the final step, the three different blocks of the Kohn−Sham matrix F^{tot} are diagonalized separately. Denoting the matrices of right eigenvectors for the three subspaces as U_L, U_M, and U_R, respectively, the Kohn−Sham matrix is transformed to the new basis of eigenvectors

$$\overline{F} = U^T F^{tot} U = \begin{pmatrix} E_L & V_{LM} & V_{LR} \\ V_{ML} & E_M & V_{MR} \\ V_{RL} & V_{RM} & E_R \end{pmatrix} \quad (2.19)$$

where

$$U = \begin{pmatrix} U_L & 0 & 0 \\ 0 & U_M & 0 \\ 0 & 0 & U_R \end{pmatrix} \quad (2.20)$$

The elements of the thus transformed Kohn–Sham matrix $\bar{F}$ determine the electronic parameters of the model Hamiltonian (2.13): The diagonal submatrices E_L and E_R contain the lead energies E_k, the diagonal submatrix E_M contains the eigenenergies of the molecular bridge and the submatrices V describe the electronic coupling matrix elements V_{km} between states localized on the leads and the molecule. In all our model systems, the distance between the two metal clusters is relatively large. Therefore, direct lead–lead coupling was small enough to be neglected.

The electronic states in the Hamiltonian (2.13) can be identified with the eigenstates of the three different blocks of the Kohn–Sham matrix and are related to the original atomic orbital basis via

$$|\phi_\alpha\rangle = \sum_{n,l} U_{\alpha n}(S^{-1/2})_{nl}|\chi_l\rangle \quad (2.21)$$

where $\alpha \in L$, M, and R. Although the eigenvectors of F_M^{tot}, $|\phi_m\rangle$ form an orthogonal basis in molecular space, the eigenvectors of the non-Hermitian matrix F_L^{tot}, $|\phi_k\rangle$, form a biorthogonal basis in the left lead space. Their overlap, $\langle \phi_k | \phi_{k'} \rangle = S_k^U \delta_{kk'}$, where $|\phi_k\rangle$ is the right eigenvector of F_L^{tot} and $\langle \phi_k|$ is its transposed, is in general a complex number. The same is true for the right lead space. We note that a similar separation scheme was employed in the study of electron transfer dynamics in dye-semiconductor systems.[56]

3. Nuclear Parameters. To characterize the nuclear degrees of freedom of the molecular bridge and determine the corresponding parameters in the Hamiltonian (2.13) a normal-mode analysis on an extended molecule including two gold layers (i.e., five gold atoms on each side) was performed. Thereby, the atomic mass of the gold atoms was set to 10^9 atomic mass units to separate the nuclear motion in the molecular bridge from that of the gold clusters.

The electronic-nuclear coupling constants $\kappa_l^{(m)}$ were obtained from the numerical gradients of the energies E_m with respect to the dimensionless normal coordinates q_l,

$$\kappa_l^{(m)} = \frac{E_m(+\Delta q_l) - E_m(-\Delta q_l)}{2\Delta q_l} \quad (2.22)$$

To this end, two DFT calculations with molecular geometries elongated by $\pm\Delta q_l = \pm 0.1$ from the equilibrium geometry were performed. The value of $\Delta q_l = 0.1$ was chosen based on convergence tests.

C. Observables of Interest. Several observables are of interest to characterize the effects of vibrational motion on charge transport through single molecule junctions. Here, we will focus on the inelastic transmission probability, which describes the transmission process of a single electron or hole through the molecular junction and the current–voltage characteristics. In all of the examples considered below, the transport is dominated by hole transport. The inelastic transmission probability of a single hole from the left to the right lead as a function of initial and final energy of the hole is given by the expression

$$T_{R \leftarrow L}(E_i, E_f) = 4\pi^2 \sum_{\nu_i, \nu_f} \sum_{k_i \in L} \sum_{k_f \in R} P_{\nu_i} \delta(E_{\nu_f} - E_f - E_{\nu_i} + E_i) \times$$

$$\delta(E_i - E_{k_i})\delta(E_f - E_{k_f})|\langle \nu_f | \langle k_f | VG(E)V | k_i \rangle | \nu_i \rangle|^2 \quad (2.23)$$

Here, the δ-function accounts for energy conservation, $E \equiv E_{\nu_i} - E_i = E_{\nu_f} - E_f$ with E_{ν_i} and E_{ν_f} being the energy of the initial and final vibrational states $|\nu_i\rangle, |\nu_f\rangle$, respectively, $-E_i$ and $-E_f$ are the initial and final energies of the hole, and $G(E) = (E^+ - H)^{-1}$ is the Green's function. The latter is defined with respect to the model Hamiltonian (2.13), the parameters of which have been determined from first principles as described in section II.B.2. Furthermore, $P_{\nu_i} = \langle \nu_i | \rho_0 | \nu_i \rangle$ denotes the population probability of the initial vibrational state, $\rho_0 = e^{-H_{n0}/(k_B T)}/Z$. In the systems considered in this work, the hole couples primarily to modes with relatively high frequencies. As a result, thermal effects are not expected to be of relevance and the initial vibrational state is assumed to be the ground state, i.e., $\rho_0 = |0\rangle\langle 0|$. The total transmission probability, $T_{R \leftarrow L}(E_i)$, is obtained by integrating $T_{R \leftarrow L}(E_i, E_f)$ over the total range of final energies of the hole

$$T_{R \leftarrow L}(E_i) = \int dE_f \, T_{R \leftarrow L}(E_i, E_f) \quad (2.24)$$

To calculate the transmission probability, the Green function $G(E)$ in the expression for the transmission probability is projected onto the molecular space using the projection operators $P = \sum_{m \in M} |\phi_m\rangle\langle\phi_m|$, $Q_L = \sum_{k \in L} |\phi_k\rangle\langle\phi_k|$, $Q_R = \sum_{k \in R} |\phi_k\rangle\langle\phi_k|$, as well as the Lippmann–Schwinger equation $G = G_0 + G_0 VG$. This results in the expression

$$T_{R \leftarrow L}(E_i, E_f) = \sum_{\nu_i, \nu_f} P_{\nu_i} \delta(E_{\nu_f} - E_f - E_{\nu_i} + E_i) \times$$

$$tr_M\{\langle \nu_i | \Gamma_L(-E_i)G_M^\dagger(E_{\nu_i} - E_i)|\nu_f\rangle\langle\nu_f|\Gamma_R(-E_f)G_M(E_{\nu_i} - E_i)|\nu_f\rangle\} \quad (2.25)$$

where the trace is taken over the electronic states on the molecule (M) and the Green's function projected onto the molecular bridge is given by

$$G_M(E) = PG(E)P$$

$$= [E^+ - PHP - \Sigma_L^{lead}(E - H_{n0}) - \Sigma_R^{lead}(E - H_{n0})]^{-1}$$

$$= [E^+ + H_M - H_{n0} + H_{ne} -$$

$$\Sigma_L^{lead}(E - H_{n0}) - \Sigma_R^{lead}(E - H_{n0})]^{-1} \quad (2.26)$$

Here, $\Sigma_{L/R}^{lead}(E)$ denote the self-energy due to coupling to the left and right lead, respectively

$$\Sigma_L^{lead}(E) = PVQ_L(E^+ + H_L)^{-1}Q_L VP = -\frac{i}{2}\Gamma_L(E) + \Delta_L(E) \quad (2.27a)$$

$$\Sigma_R^{lead}(E) = PVQ_R(E^+ + H_R)^{-1}Q_R VP = -\frac{i}{2}\Gamma_R(E) + \Delta_R(E) \quad (2.27b)$$

where $\Gamma_L(E)$ and $\Delta_L(E)$ are the corresponding width and level-shift functions. The matrix elements of the self-energy in the molecular space are given by

$$\left(\Sigma_L^{lead}(E)\right)_{mn} = \sum_k \frac{V_{km}V_{nk}}{(E^+ + E_k)} \quad (2.28)$$

It should be emphasized that the thus defined self-energy $\Sigma_L^{lead}(E)$ corresponds to hole transport. It is related to the commonly used self-energy for electron transport, $\Sigma_{el\,L}^{lead}(E)$ via

$$\left(\Sigma_L^{lead}(E)\right)_{mn} = -\left(\Sigma_{el\,L}^{lead}(-E)\right)_{mn}^* \quad (2.29)$$

In the practical calculations, the latter self-energy is obtained using the partitioning method outlined above and is explicitly given by

Vibronic Effects in Single Molecule Conductance

J. Phys. Chem. C, Vol. 112, No. 26, 2008 **9885**

$$\left(\Sigma_{\text{el L}}^{\text{lead}}(E)\right)_{mn} = \sum_k \frac{V_{mk}V_{kn}}{S_k^U(E^+ - E_k)} \quad (2.30)$$

and analogously for $\Sigma_{\text{el R}}^{\text{lead}}$. The appearance of the overlap factor S_k^U in eq 2.30 is a consequence of the biorthogonal basis on the leads (cf. the discussion in section II.B 2).

It is noted that, in contrast to purely electronic transport calculations as well as applications of the nonequilibrium Green's function formalism to vibronic transport,[26,59] the Green's function G_M and the self-energies Σ_L^{lead}, Σ_R^{lead} in eq 2.26 are operators with respect to both the electronic and nuclear degrees of freedom. Thus, the Green's function has to be evaluated in the combined electronic-vibrational Hilbert space. In the calculations reported below, the Green's function G_M is obtained by inverting a basis representation of the operator $E^+ - PHP - \Sigma_L^{\text{lead}}(E - H_{n0}) - \Sigma_R^{\text{lead}}(E - H_{n0})$ for each energy E employing a harmonic oscillator basis for the vibrational modes.

Based on the transmission probability (eq 2.25), the current through the molecular junction is obtained using a generalized Landauer formula[60]

$$I = \frac{2e}{h} \int dE_i \int dE_f \{T_{R \leftarrow L}(E_i, E_f)f_R(E_f)[1 - f_L(E_i)] -$$

$$T_{L \leftarrow R}(E_i, E_f)f_L(E_f)[1 - f_R(E_i)]\} \quad (2.31)$$

where $f_L(E)$ and $f_R(E)$ denote the Fermi distribution for the left and the right lead, respectively, taken at zero temperature.

Although eqs 2.23 and 2.25 for the single-hole transmission probability involve no approximation, expression 2.31 for the current is only valid if many-body processes are of minor importance. In particular, nonequilibrium effects in the leads and electron correlation due to electronic−vibrational coupling are not taken into account. Furthermore, it is implicitly assumed, that the nuclear degrees of freedom of the molecular bridge relax to the vibrational equilibrium state after scattering of a hole, e.g., by excitation of electron−hole pairs. It is also noted that the scattering theory approach used in this work can also not account for a partial occupation of the electronic states in the stationary transport regime. For the applications considered below, comparison with calculations based on nonequilibrium Green's function methods indicate that these assumptions are justified.[48] Without vibronic coupling the expression for the current, eq 2.31, reduces to the usual Landauer formula.[61]

In principle, the basis states $|\phi_m\rangle$, $|\phi_k\rangle$, the hole energies and the nuclear parameters depend on the bias voltage. For the studies in this work, we did not include the voltage self-consistently in the DFT calculation but used, for simplicity, parameters obtained from electronic-structure calculations at equilibrium and assumed that the bias voltage V enters the formulas only via the chemical potentials of the leads $\mu_{L/R} = \varepsilon_f \pm eV/2$, where ε_f denotes the Fermi energy. The energies of the lead states for finite voltage are thus given by $E_k \pm eV/2$. Since we do not invoke the wide-band approximation, the Green's function G_M, the self-energies $\Sigma_{L/R}^{\text{lead}}$ as well as the width functions $\Gamma_{L/R}$ also depend on the bias voltage.

III. Results and Discussion

The theoretical methodology outlined above has been applied to study vibrational effects in electron transport through the three different molecular junctions depicted in Figure 1, which include benzene-di(ethanethiolate) (BDET) between pyramidal and cuboid-shaped gold contacts as well as benzene-di(butanethiolate) (BDBT) with a pyramidal contact geometry. To reduce the computational effort, in the calculations presented below,
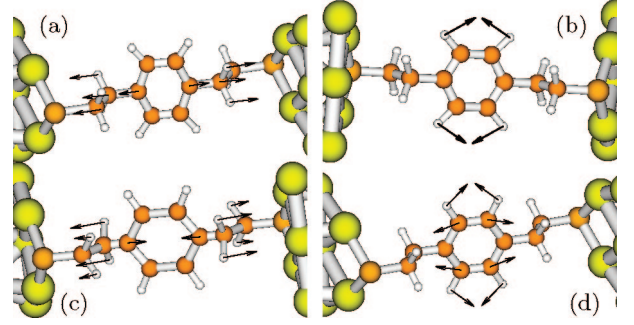

Figure 2. Normal modes of BDET included in the calculation.

TABLE 1: Parameters of the Four Most Important Vibrational Modes of BDET between Pyramidal Gold Contacts Including Frequencies, Periods, and Vibronic Coupling in the Electronic States A and B

	ω (cm^{-1})	T (fs)	κ^A (meV)	κ^B (meV)
(a)	544.48	61	76	22
(b)	1197.11	28	51	69
(c)	1229.49	27	110	47
(d)	1671.56	20	136	162

the four vibrational modes with the strongest vibronic coupling (as determined by the ratio of the electronic-vibrational coupling κ and the electronic coupling Γ) were explicitly taken into account. Furthermore, the number of electronic states $|\phi_m\rangle$ on the molecular bridge, which were explicitly included in the calculation, was reduced by including only those with energies in the vicinity of the Fermi energy (12 for BDET and 6 for BDBT).

A. Benzene-di(ethanethiolate) with a Pyramidal Gold Cluster Geometry. We first consider the transport characteristics of BDET between two pyramidal gold clusters (Figure 1, top panel). Figure 2 depicts the four vibrational normal modes of BDET with the strongest vibronic coupling included in the calculation, which can be characterized as C−C−C bending (a and c), C−C−H bending (b), and C−C stretching (d). The corresponding normal-mode frequencies and vibronic coupling constants in the two most important molecular orbitals are given in Table 1.

The transmission probability of BDET at zero voltage is depicted in Figure 3a. In addition to the transmission probability based on a vibronic calculation, also the result of a purely electronic calculation (where all vibronic coupling constants $\kappa_i^{(m)}$ have been set to zero) is shown. The result of the purely electronic calculation exhibits two pronounced resonance peaks at energies −2.23 and −1.85 eV. These two resonances are the closest to the Fermi energy and thus determine the transport process. The two resonances are caused by the orbitals A and B depicted in Figure 3a. Assuming that the projected molecular space includes the same number of electron pairs as in the isolated molecule, the states A and B would correspond to the HOMO-4 and HOMO-5 of the isolated molecule. While orbital A resembles an e_{1g} orbital of benzene, orbital B has additional contributions on the ethyl-groups and the sulfur atoms. As a consequence, state A has smaller electronic coupling to the leads ($\Gamma_{AA} = 1.9 \times 10^{-4}$ eV, corresponding to a lifetime of $\tau = \hbar/\Gamma_{AA} = 3466$ fs) resulting in a very narrow peak in the transmission probability, whereas the significant coupling of orbital B to the leads ($\Gamma_{BB} = 1.1 \times 10^{-1}$ eV, corresponding to a lifetime of $\tau = 6$ fs) results in a rather broad structure. It is noted that, in this estimate of the lifetime, the width function Γ has been taken at the corresponding resonance peak energy. Due to the
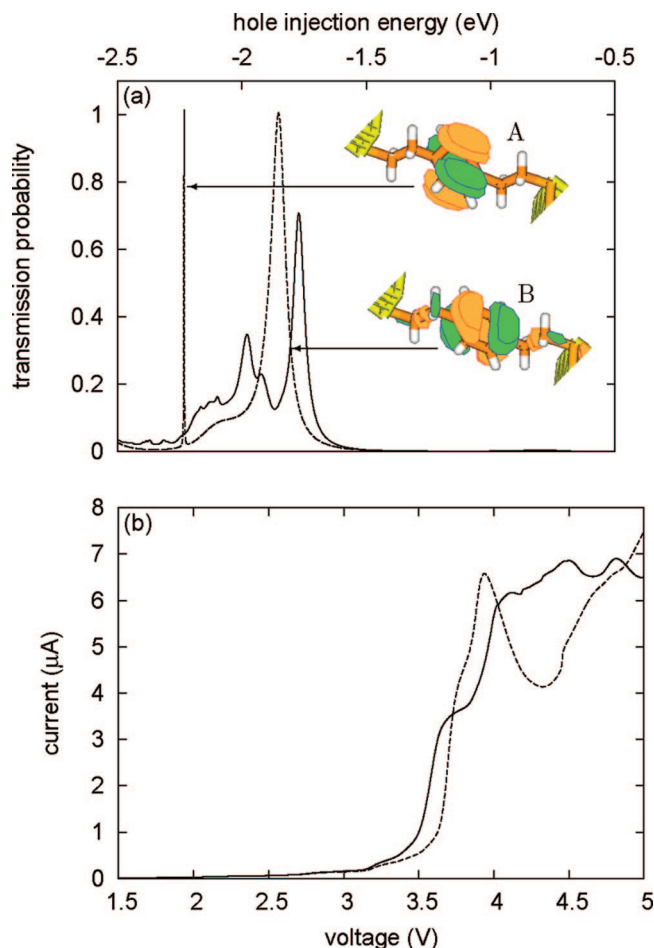
Figure 3. (a) Total transmission probability through a BDET molecular junction with a pyramidal gold cluster geometry at zero voltage as a function of the initial energy of the hole (relative to the Fermi energy). The two orbitals, denoted A and B, dominate the transmittance at the indicated peaks. Only the energy range with nonzero transmittance in the interval $[-2.5:+2.5]$, corresponding to a voltage window of 5 V, is shown. (b) Current−voltage characteristic of BDET bound to pyramidal gold contacts. Only the nonzero part of the positive voltage range is shown. The different lines in the two panels show results of calculations with (dashed line) and without (solid line) vibronic coupling.

interaction with the leads and neighboring states, the peak energy, in general, does not coincide with eigenenergies of the states after projection, E_m. For example, there exist four pairwise degenerate sulfur p states with energies close to the Fermi level, which do not appear themselves in the transmission probability but influence the transmission via their interaction with states A and B. This interaction is mediated by the gold clusters via the nondiagonal elements in the self-energy matrix.

The comparison between the results of vibronic (solid line in Figure 3a) and purely electronic (dashed line) calculations demonstrates that the electronic-vibrational coupling in BDET alters the transmission probability noticeably. In particular, it results in a shift of the electronic resonance peaks due to nuclear relaxation and the appearance of new structures, which correspond to vibrational states in the molecular cation. Specifically, the electronic resonance of state B is shifted by 0.08 eV to the peak corresponding to the 0_0^0 transition[62] and the transmission shows resonance structures at -1.92 and -1.98 eV corresponding to single vibrational excitations of mode (b) ($(\nu_b)_0^1$ transition) and (d) ($(\nu_c)_0^1$ transition). It is noted that in contrast to previous calculations,[43] where charge transport through BDET was

described as electron instead of hole transport, the shift due to nuclear relaxation is in the opposite direction and the higher excited vibrational states in the vibrational progressions are located at lower energies. The 0_0^0 transition peak belonging to state A, which may be expected to be a narrow line, cannot be seen because it is coincidentally shifted into resonance with a sulfur p-state transmission peak. This peak, which does not appear directly in the transmission probability, causes a broadening of the resonance of state A. The structure resulting from this effect can be seen around peak A, but it is too broad to assign individual modes.

The current−voltage characteristic of BDET is shown in Figure 3b. Due to the symmetry of the junctions, the current fulfills the relation $I(-V) = -I(V)$, and therefore, only the positive voltage range is shown. The result obtained from a purely electronic calculation (dashed line) shows an increase of the current at about 3.5 V related to hole transport through state B. The increase is followed by a pronounced decrease of the current at 4 V. This negative-differential resistance (NDR) effect is a result of the voltage dependence of the self-energies Σ_L^{lead} and Σ_R^{lead} and the corresponding width functions Γ and will be discussed in more detail below. The weakly coupled state A results only in a small step-like increase of the current shortly before 4.5 V and the following rise of the current is due to the increasing width of the resonance peak due to state B which appears at -1.85 eV in the transmission probability.

Including the coupling to the nuclear degrees of freedom changes the current−voltage characteristic significantly. In particular, the electronic-vibrational coupling results in an earlier onset of the current, a quenching of the NDR effect as well as step-like substructures which can be associated with vibrational excitation in the B state. The earlier onset of the current is due to the fact that upon interaction with vibrations the resonance peaks are shifted to higher energies and thus enter the voltage window at lower voltage. If the voltage window is large enough to comprise all vibronic features, the difference between purely electronic and vibronic results for the current vanishes. The vibrational substructures are a result of the splitting of each electronic resonance into several vibronic resonances (cf. Figure 3a), which contribute with different weights (determined by the respective Franck−Condon factors) to the transmission. In contrast to the purely electronic case, the current thus increases in several steps. This effect is well-known from previous model studies.[36,40]

Smaller structures in the current−voltage characteristics are more clearly revealed in the differential conductance, dI/dV. Figure 4 shows the differential conductance of BDET obtained by numerical differentiation of the current in Figure 3b. Overall, the differential conductance reflects the transmittance of the junction. However, in contrast to the transmission probability at zero voltage (depicted in Figure 3a), it also incorporates its voltage dependence and the effects of the Fermi distribution in the leads. In the purely electronic conductance (dashed line), this difference manifests itself in the splitting of the peak due to state B as well as the negative differential resistance between 4 and 4.3 V. At 4.5 V a narrow resonance due to state A can be seen. The differential conductance based on the vibronic calculation exhibits pronounced structures due to vibronic coupling. These include the shifted onset (corresponding to the 0_0^0 transitions) of state A at 3.58 V and state B at 4.27 V as well as resonance peaks at 3.98 V corresponding the $(\nu_d)_0^1$ vibrational excitation in state B and at 4.32 V reflecting the $(\nu_a)_0^1$ excitation in state A. The differential conductance based on the vibronic calculation shows, furthermore, small regions
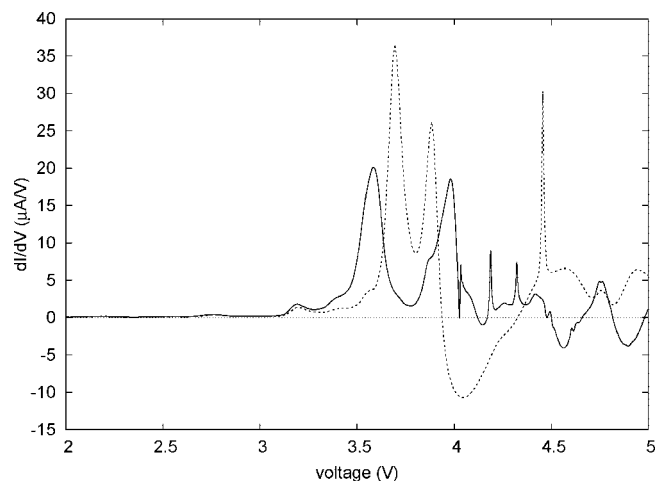
Vibronic Effects in Single Molecule Conductance

J. Phys. Chem. C, Vol. 112, No. 26, 2008 **9887**

Figure 4. Conductance of BDET based on a purely electronic (dashed line) and a vibronic (solid line) calculation.
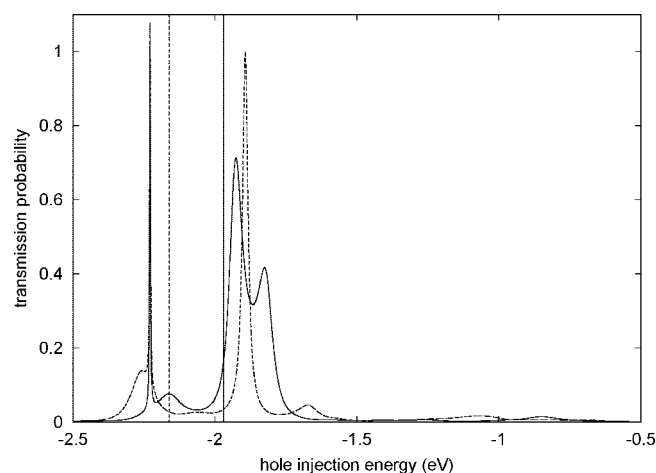

Figure 5. Transmission of BDET at voltages 3.94 (solid line) and 4.32 V (dashed line) based on a purely electronic calculation. The two vertical lines indicate the respective lower integration boundaries.

of negative differential resistance for larger voltages, which do not exist in the purely electronic differential conductance.

Finally, we consider the mechanisms responsible for the NDR effect observed in the results discussed above. As was mentioned above, the NDR effect is caused by the voltage dependence of the self-energies. These result in a voltage dependence of the transmission probability which in turn determine the current via the integral in eq 2.31. To elucidate the mechanism causing NDR in the purely electronic calculation (dashed lines in Figures 3b and 4), Figure 5 depicts the transmission probability for voltages of 3.94 V (corresponding to the local maximum in the I−V curve) and 4.32 V (the local minimum in the I−V curve). The peak caused by orbital B in the transmission for 3.94 V (dashed line) is much thinner than the corresponding peak in the curve for 4.32 V (solid line). Although the current in the former case corresponds to the integral with a lower boundary (see vertical line in Figure 5), the area under the "4.32 V" transmission curve is much smaller thus explaining the NDR in the current−voltage characteristic and the conductance. It should be emphasized that this NDR effect can only be described, if the energy and voltage dependence of the self-energies is taken into account and will be missed within the often used wide-band approximation.

B. Benzene-di(ethanethiolate) with a Cuboid-Shaped Gold-Cluster Geometry. To investigate the influence of the gold-cluster geometry on the transport properties of the molecular
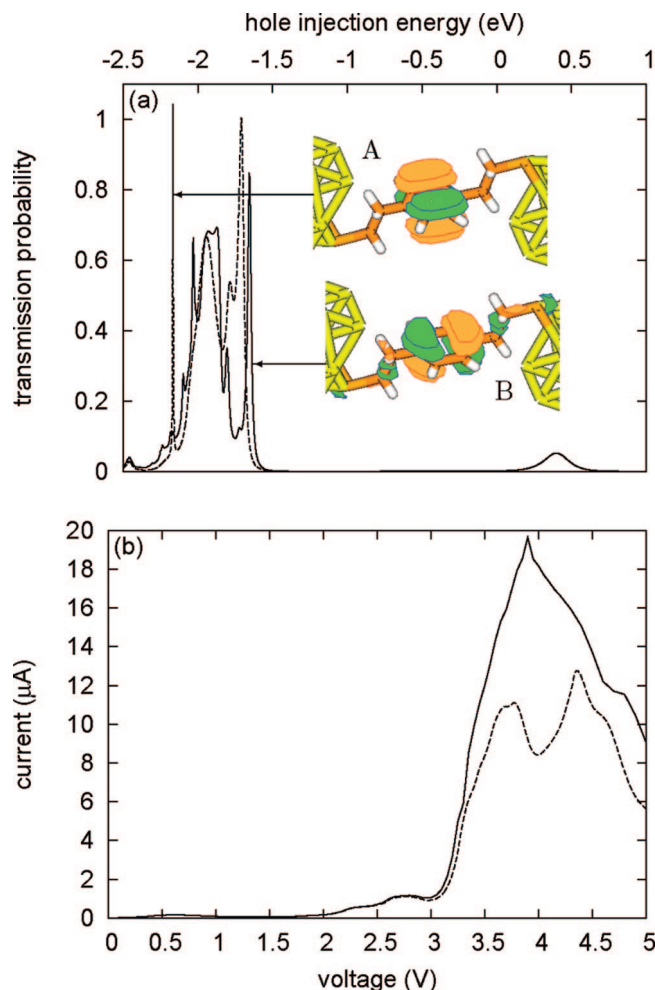

Figure 6. (a) Total transmission probability through a BDET molecular junction with a cuboid-shaped gold cluster geometry at zero voltage as a function of the initial energy of the hole (relative to the Fermi energy). The two orbitals, denoted A and B, dominate the transmittance at the indicated peaks. Only the energy range with nonzero transmittance in the interval [−2.5:+2.5], corresponding to a voltage window of 5 V, is shown. (b) Current−voltage characteristic of BDET bound to cuboid-shaped gold contacts. Only the nonzero part of the positive voltage range is shown. The different lines in the two panels show results of calculations with (dashed line) and without (solid line) vibronic coupling.

junction, we have studied a system where the molecule BDET is bound to gold-clusters with different geometry of cuboid shape (cf. Figure 1 middle panel). To build this geometry, we started from the optimized two-layer system described above. Next, the number of gold atoms in the second layer was increased from 5 to 12, and two more gold-(111) layers consisting of 12 gold atoms each were added, thus resulting in a metal cluster of 38 gold atoms on each side. For better comparison with the results obtained in section III.A, the same value was used for the Fermi energy. The four normal modes and the molecular electronic states included in the calculation are very similar to those in section III.A.

Figure 6a shows the zero-voltage transmission probability for this system. The comparison with the corresponding result for the pyramidal gold-cluster geometry (Figure 3) reveals overall a significant effect of the cluster geometry. Considering specifically the transmission based on the purely electronic calculation, the resonance due to state B is split into three peaks at −1.71, −1.79, and −1.95 eV. This is caused by the electrode-mediated interaction of state B with both lower and higher lying states,

9888 *J. Phys. Chem. C, Vol. 112, No. 26, 2008*
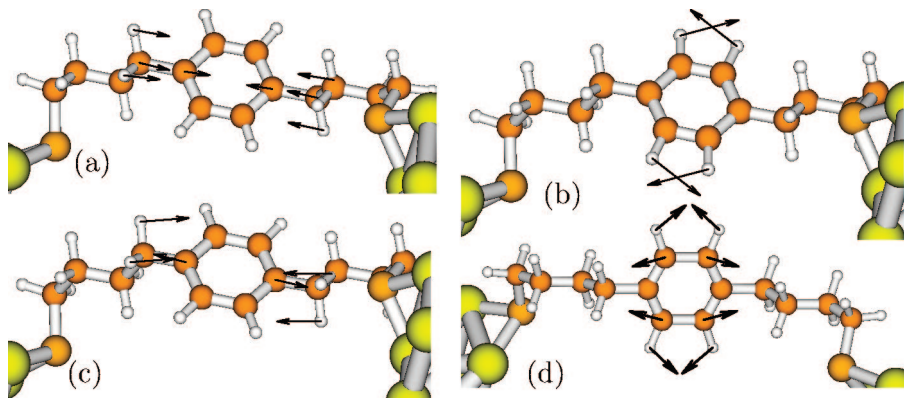
Benesch et al.

Figure 7. Normal modes of BDBT included in the calculation.

which is more pronounced in the cuboid gold-cluster geometry. In addition, there is a small broad peak at 0.39 eV due to two sulfur p orbitals, which is missing in the pyramidal geometry. The resonance due to state A in the zero-voltage transmission, on the other hand, is almost unaffected by the geometry of the gold cluster. This is to be expected because state A is exclusively localized on the benzene ring. The coupling of states A and B to the contacts is of comparable size as for the pyramidal gold clusters: $\Gamma_{AA}(-2.17) = 4.0 \times 10^{-4}$ eV (corresponding to a lifetime of $\tau = 1646$ fs), $\Gamma_{BB}(-1.98) = 6.5 \times 10^{-2}$ eV ($\tau = 10$ fs), and $\Gamma_{BB}(-1.71) = 1.1 \times 10^{-1}$ eV ($\tau = 6$ fs).

Considering the results of the vibronic calculations (full line in Figures 3, 6), the most significant difference between the two cluster geometries is the appearance of the 0_0^0 transition and vibrational progressions due to state A. These were not visible in the system with the pyramidal gold clusters due to accidental coincidences with transmission features of other states. In the system with cuboid cluster geometry, the 0_0^0 line due to state A appears at -2.03 eV and the $(\nu)_0^1$ transition peaks corresponding to all four vibrational modes can be seen at -2.10 (a), -2.17 (b), -2.18 (c), and -2.24 (d) eV.

Figure 6b shows the current−voltage characteristic for the BDET system with cuboid gold clusters. The current−voltage characteristic based on the purely electronic calculation (dashed line) has a similar appearance as in the system with the pyramidal cluster (cf. Figure 3b). Noticeable differences are the earlier onset and the overall larger value of the current as well as the appearance of two (instead of one) maxima with corresponding regions of NDR. The larger current is a manifestation of the overall larger molecule-lead coupling provided by the binding to the cuboid shaped gold cluster. The earlier onset of the current is caused by orbitals localized on the sulfur atoms. The appearance of two maxima is due to the splitting of the resonance peak of state B. We next consider the current based on the vibronic calculation (full line in Figure 6b). In contrast to the system with the pyramidal gold cluster geometry, vibrational substructures are less pronounced and the current obtained with the vibronic calculation is in some regions significantly larger than that based on the electronic current. Furthermore, NDR effects are only partly quenched by the interaction with the vibrational degrees of freedom.

To conclude this section, the comparison of the data for BDET bound to two different gold clusters shows that the geometry of the gold contact may have a significant influence on the transport properties. This is in accordance with results of ref 63, which show that the transport characteristics of benzene-di(thiol) depends on the surface structure and the lateral size of the electrodes. Our results show that the influence of

the gold contact geometry is particularly pronounced for transport through molecular orbitals which have a significant contribution at the boundary to the contacts such as state B in the system studied here. In experiments, where it is often not straightforward to control the molecule-lead binding geometry, this difference may result in fluctuations of the current for different realizations of molecular junctions.

C. Benzene-di(butanethiolate). The systems studied in the previous sections are characterized by a moderate molecule-lead coupling, corresponding to a relatively short lifetime of the electron on the molecular bridge. Accordingly, vibrational effects are noticeable but not very pronounced. The coupling between the π system of the molecular bridge and the gold electrodes can be reduced (and thus the lifetime of the electron on the bridge extended) by increasing the length of the alkyl-spacer group. As an example of such a system, we consider in this section electron transport through *p*-benzene-di(butanethiolate) (BDBT) (cf. Figure 1, bottom panel). Thereby, the contacts were modeled with a gold cluster of pyramidal geometry. The transport properties of this system can be well described including six electronic states localized at the molecular bridge in the calculation. These comprise the states A and B illustrated in Figure 8, which are similar as in BDET, and four sulfur p orbitals. As in the previous system, from all 54 totally symmetric normal modes the four with the strongest vibronic coupling were included explicitly in the calculation. The modes are depicted in Figure 7. Their frequencies and coupling constants are given in Table 2.

Figure 8a shows the zero-voltage transmission probability of BDBT. In contrast to BDET, the transmission probability exhibits well-separated narrow resonance structures. This is due to the significantly smaller electronic coupling. The results based on the purely electronic calculation exhibit two narrow resonances at -1.78 and -1.39 eV. These are due to states A and B, respectively, which couple to the gold electrodes with coupling strengths of $\Gamma_{AA}(-1.78) = 1.0 \times 10^{-3}$ eV ($\tau = 659$ fs) and $\Gamma_{BB}(-1.39) = 5.4 \times 10^{-4}$ eV ($\tau = 1220$ fs), respectively. Due to the small coupling, these states exhibit negligible level shift. Including vibronic coupling both peaks are shifted to the respective 0_0^0 transition and pronounced vibrational progressions appear. The individual peak heights correspond to the respective Franck−Condon factors. Table 3 gives an assignment of the most prominent resonances.

The current−voltage characteristic of BDBT is depicted in Figure 8b. The result based on the purely electronic calculation shows two prominent steps corresponding to states A and B at voltages 2.76 and 3.56 V, respectively. In addition, there is a small current for low voltages and another step-like structure
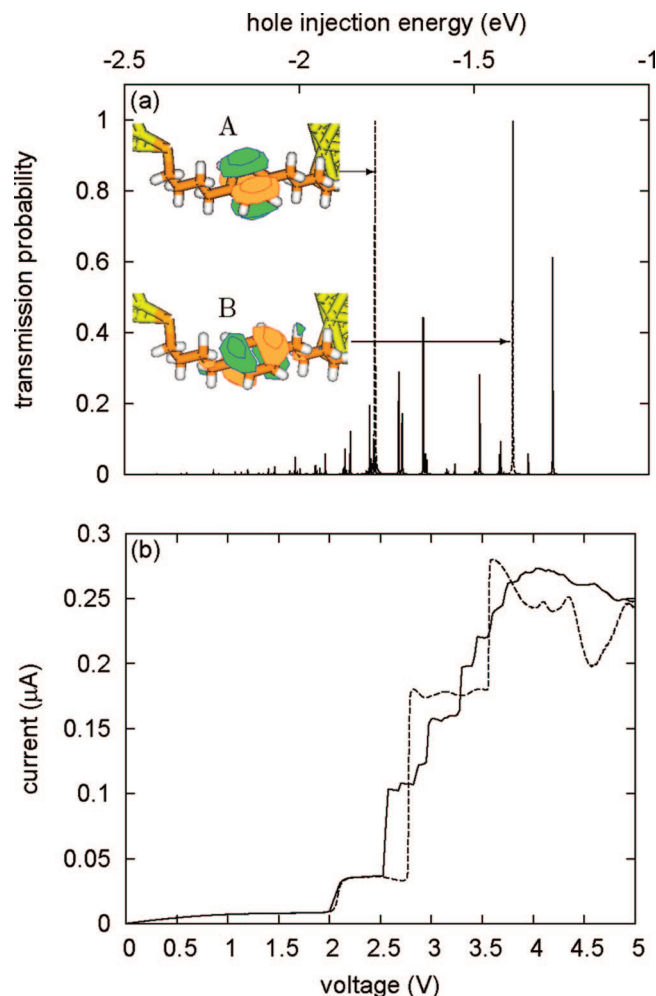
Vibronic Effects in Single Molecule Conductance

J. Phys. Chem. C, Vol. 112, No. 26, 2008 **9889**

Figure 8. (a) Total transmission probability through a BDBT molecular junction with a pyramidal gold cluster geometry at zero voltage as a function of the initial energy of the hole (relative to the Fermi energy). The two orbitals, denoted A and B, dominate the transmittance at the indicated peaks. Only the energy range with nonzero transmittance in the interval $[-2.5:+2.5]$, corresponding to a voltage window of 5 V, is shown. (b) Current−voltage characteristic of BDBT bound to pyramidal gold contacts. Only the nonzero part of the positive voltage range is shown. The different lines in the two panels show results of calculations with (dashed line) and without (solid line) vibronic coupling.

TABLE 2: Parameters of the Four Most Important Vibrational Modes of BDBT between Pyramidal Gold Contacts Including Frequencies, Periods, and Vibronic Coupling in the Electronic States A and B

	ω (cm^{-1})	T (fs)	κ^A (meV)	κ^B (meV)
(a)	566.12	59	69	29
(b)	1198.40	28	52	73
(c)	1232.90	27	114	56
(d)	1676.10	20	132	170

at 2 V. Both features are due to sulfur p-states, which cause a small but very broad peak in the transmission probability around the Fermi level and a small, narrow peak at -1 eV, which can be seen in the transmission probability at 2 V only (data not shown), but not in the zero-voltage transmission. As in the other model systems, NDR effects caused by the same mechanism as for BDET appear at larger voltages. Upon including vibronic coupling, the onset of the current related to states A and B is shifted to lower voltage due to nuclear relaxation. Furthermore, a number of additional steplike structures appear which can be

TABLE 3: Assignments of the Most Pronounced Vibronic Transitions in the Transmission Function of BDBT Depicted in Figure 8a[a]

orbital A	$(\nu)_0^1$	$(\nu)_0^2$
mode (a)	−1.72	−1.79
mode (b)		
mode (c)	−1.80	−1.93
mode (d)	−1.85	−2.07

orbital B	$(\nu)_0^1$	$(\nu)_0^2$
mode (a)	−1.35	
mode (b)	−1.42	−1.56
mode (c)	−1.43	
mode (d)	−1.48	−1.71

[a] The locations of the features are given in eV. Blank entries correspond to transitions that could not be identified because of too small vibronic coupling.

TABLE 4: Assignments of the Most Pronounced Vibronic Transitions in the I−V Curve of BDBT Depicted in Figure 8b[a]

	orbital A	orbital B
0_0^0	3.27	2.55
$(\nu_a)_0^1$	3.42	2.68
$(\nu_b)_0^1$	3.57	2.85
$(\nu_c)_0^1$	3.57	2.85
$(\nu_d)_0^1$	3.73	2.95
$(\nu_d)_0^2$		3.42

[a] The location of the features are given in V. Blank entries correspond to transitions that could not be identified, because of too small vibronic coupling.

assigned to excitation of the different vibrational modes in states A and B. The most pronounced features are analyzed in Table 4. The NDR following the last step still exists but is significantly smaller compared to the purely electronic case.

IV. Conclusions

In this paper we have studied the effect of vibrational motion on resonant charge transport in single molecule junctions. The methodology used to describe vibrationally coupled charge transport is based on a combination of first-principles electronic structure calculations to characterize the system and inelastic scattering theory. To apply this methodology to systems where the transport is dominated by the occupied molecular orbitals of the junction, we have extended the approach to allow for hole transport.

We have applied the methodology to molecular junctions where a benzene molecule is connected via alkanethiol bridges to two gold electrodes. This class of molecular junctions was chosen, because the change of the length of the alkyl chain allows a systematic variation of the coupling between the π system of the phenyl ring and the gold electrodes and thus a variation of the lifetime of the electron on the molecular bridge. The ratio between the vibronic coupling and the electronic molecule-lead coupling determines the importance of vibronic effects in molecular junctions. The results of this study demonstrate this trend. Our previous work[43] had indicated that in benzene-di(thiolate), which is characterized by rather strong molecule-lead coupling (and thus a very short lifetime of the electron on the molecular bridge), vibrational effects in resonant transport are almost negligible. Benzene-di(butanthiolate), the system with the smallest molecule-lead coupling investigated, exhibits pronounced vibronic effects. In particular, electronic-

vibrational coupling result in a splitting of electronic resonances into vibronic subresonances in the transmission probability. In the current−voltage characteristic, vibronic effects manifest themselves in steplike structures, which can be associated with vibrational states in the molecular cation. Benzene-di(ethanethi-olate) is an intermediate case, which shows noticeable though not very pronounced vibronic effects. The study also shows that electronic-vibrational coupling may result in a quenching of negative differential resistance effects, which are caused by the voltage dependence of the self-energies, and a significantly altered overall magnitude of the current.

References and Notes

(1) Reed, M.; Zhou, C.; Muller, C.; Burgin, T.; Tour, J. *Science* **1997**, *278*, 252.

(2) Park, H.; Park, J.; Lim, A.; Anderson, E.; Alivisatos, A.; McEuen, P. *Nature (London)* **2000**, *407*, 57.

(3) Smit, R.; Noat, Y.; Untiedt, C.; Lang, N.; van Hemert, M.; van Ruitenbeek, J. *Nature (London)* **2002**, *419*, 906.

(4) Weber, H. B.; Reichert, J.; Weigend, F.; Ochs, R.; Beckmann, D.; Mayor, M.; Ahlrichs, R.; v.; Löhneysen, H. *Chem. Phys.* **2002**, *281*, 113–125.

(5) Xiao, X.; Xu, B.; Tao, N. *Nano Lett.* **2004**, *4*, 267.

(6) Qiu, X.; Nazin, G.; Ho, W. *Phys. Rev. Lett.* **2004**, *92*, 206102.

(7) Liu, N.; Pradhan, N.; Ho, W. J. *Chem. Phys.* **2004**, *120*, 11371.

(8) Tao, N. J. *Nat. Nano.* **2006**, *1*, 173.

(9) Chen, F.; Hihath, J.; Huang, Z.; Li, X.; Tao, N. *Annu. Rev. Phys. Chem.* **2007**, *58*, 535.

(10) Hänggi, P., Ratner, M. S. Y., Eds.; *Chem. Phys.* 281, special issue on "Processes in molecular wires".

(11) Nitzan, A.; Ratner, M. *Science* **2003**, *300*, 1384.

(12) Cuniberti, G.; Fagas, G.; Richter, K. *Introducing Molecular Electronics*; Springer: Heidelberg, 2005.

(13) Gaudioso, J.; Lauhon, L. J.; Ho, W. *Phys. Rev. Lett.* **2000**, *85*, 1918.

(14) Thijssen, W. H. A.; Djukic, D.; Otte, A. F.; Bremmer, R. H.; van Ruitenbeek, J. M. *Phys. Rev. Lett.* **2006**, *97*, 226806.

(15) Djukic, D.; Thygesen, K. S.; Untiedt, C.; Smit, R. H. M.; Jacobsen, K. W.; van Ruitenbeek, J. M. *Phys. Rev. B* **2005**, *71*, 161402.

(16) Böhler, T.; Edtbauer, A.; Scheer, E. *Phys. Rev. B* **2007**, *76*, 125432.

(17) Parks, J.; Champagne, A.; Hutchison, G.; Flores-Torres, S.; Abruna, H.; Ralph, D. *Phys. Rev. Lett.* **2007**, *99*, 026601.

(18) Pasupathy, A. N.; Park, J.; Chang, C.; Soldatov, A. V.; Lebedkin, S.; Bialczak, R. C.; Grose, J. E.; Donev, L. A. K.; Sethna, J. P.; Ralph, D. C.; McEuen, P. L. *Nano Lett.* **2005**, *5* (2), n/a.

(19) Ogawa, N.; Mikaelian, G.; Ho, W. *Phys. Rev. Lett.* **2007**, *98*, 166103.

(20) Gaudioso, J.; Ho, W. J. *Am. Chem. Soc.* **2001**, *123*, 10095–10098.

(21) Kushmerick, J.; Lazorcik, J.; Patterson, C.; Shashidhar, R.; Seferos, D. S.; Bazan, G. C. *Nano Lett.* **2004**, *4*, 639.

(22) Galperin, M.; Ratner, M. A.; Nitzan, A. J. *Phys.: Condens. Matter* **2007**, *19*, 103201.

(23) Gagliardi, A.; Solomon, G.; Pecchia, A.; Frauenheim, T.; Di, A. C.; Reimers, J.; Hush, N. *Phys. Rev. B* **2007**, *75*, 174306.

(24) Sergueev, N.; Demkov, A.; Guo, H. *Phys. Rev. B* **2007**, *75*, 233418.

(25) Mitra, A.; Aleiner, I.; Millis, A. J. *Phys. Rev. B* **2007**, *75*, 233418.

(26) Pecchia, A.; Carlo, A. D. *Nano Lett.* **2004**, *4*, 2109.

(27) Chen, Y.; Zwolak, M.; Ventra, M. D. *Nano Lett.* **2005**, *5*, 813.

(28) Frederiksen, T.; Paulsson, M.; Brandbyge, M.; Jauho, A. *Phys. Rev. B* **2007**, *75*, 205413.

(29) Troisi, A.; Ratner, M. A.; Nitzan, A. J. *Chem. Phys.* **2003**, *118*, 6072.

(30) Jiang, J.; Kula, M.; Luo, Y. J. *Chem. Phys.* **2006**, *124*, 34708.

(31) Galperin, M.; Ratner, M.; Nitzan, A. *Phys. Rev. B* **2006**, *73*, 045314.

(32) Emberly, E.; Kirczenow, G. *Phys. Rev. B* **2000**, *61*, 5740.

(33) Boese, D.; Schoeller, H. *Europhys. Lett.* **2001**, *54*, 668.

(34) May, V.; Kühn, O. *Chem. Phys. Lett.* **2006**, *420*, 192–198.

(35) Lehmann, J.; Kohler, S.; May, V.; Hänggi, P. J. *Chem. Phys.* **2004**, *121*, 2278.

(36) Koch, J.; von Oppen, F. *Phys. Rev. Lett.* **2005**, *94*, 206804.

(37) Nowack, K.; Wegewijs, M. cond-mat/0506552.

(38) Bonca, J.; Trugman, S. A. *Phys. Rev. Lett.* **1995**, *75*, 2566.

(39) Ness, H.; Shevlin, S.; Fisher, A. *Phys. Rev. B* **2001**, *63*, 125422.

(40) Cizek, M.; Thoss, M.; Domcke, W. *Phys. Rev. B* **2004**, *70*, 125406.

(41) Cizek, M.; Thoss, M.; Domcke, W. *Czech. J. Phys.* **2005**, *55*, 189.

(42) Domcke, W. *Phys. Rep.* **1991**, *208*, 97.

(43) Benesch, C.; Cizek, M.; Thoss, M.; Domcke, W. *Chem. Phys. Lett.* **2006**, *430*, 355.

(44) Cederbaum, L.; Domcke, W. J. *Chem. Phys.* **1974**, *60*, 2678.

(45) Reference 44 outlines how correlation and orbital relaxation effects can be included in the Hamiltonian.

(46) Cizek, M. to be published.

(47) For a treatment of molecular conductance including the dependence of V_{mk} on the nuclear coordinates, see ref 64.

(48) Härtle, R.; Benesch, C.; Thoss, M. *Phys. Rev. B* **2008**, *77*, 205314.

(49) Ahlrichs, R.; Bär, M.; Häser, M.; Horn, H.; Kölmel, C. *Chem. Phys. Lett.* **1989**, *162*, 165.

(50) Basch, H.; Ratner, M. A. J. *Chem. Phys.* **2003**, *119*, 11926.

(51) Kurnikov, L.; Beratan, D. J. *Chem. Phys.* **1996**, *105*, 9561.

(52) Galperin, M.; Toledo, S.; Nitzan, A. J. *Chem. Phys.* **2002**, *117*, 10817.

(53) Löwdin, P.-O. J. *Chem. Phys.* **1950**, *18*, 365.

(54) Mayer, I. *Int. J. Quantum Chem.* **2002**, *90*, 63.

(55) Klimes, J. Master's thesis; Charles University: Prague.

(56) Kondov, I.; Cizek, M.; Benesch, C.; Wang, H.; Thoss, M. J. *Phys. Chem. C* **2007**, *111*, 11970–11981.

(57) Lopez Sancho, M.; Lopez Sancho, J.; Rubio, J. J. *Phys. F: Met. Phys.* **1985**, *15*, 851.

(58) Mehl, M.; Papaconstantopoulos, D. *Phys. Rev. B* **1996**, *54*, 4519.

(59) Ryndyk, D. A.; Hartung, M.; Cuniberti, G. *Phys. Rev. B* **2006**, *73*, 045420.

(60) Nitzan, A. *Annu. Rev. Phys. Chem.* **2001**, *52*, 681–750.

(61) Meir, Y.; Wingreen, N. *Phys. Rev. Lett.* **1992**, *68*, 2512.

(62) Here, we are using spectroscopic notation $(\nu)_n^l$ to denote vibronic transitions of mode ν from the nth vibrational state in the neutral molecule to the lth vibrational state in the molecular cation. 0_0^0 denotes the transition between the respective vibrational ground states.

(63) Ke, S.; Baranger, H. U.; Yang, W. J. *Chem. Phys.* **2005**, *123*, 114701.

(64) Caspary-Toroker, M.; Peskin, U. J. *Chem. Phys.* **2007**, *127*, 154706.

JP711940N